Numerical Investigation of Heat Transfer in Straight Pipe of Elliptic Cross-Section Rotating in Orthogonal Mode

O. T. Popoola*, O. A. Lasode, I. K. Adegun, A. B. Rabiu

Department of Mechanical Engineering, Faculty of Engineering and Technology, University of Ilorin, PMB 1515, Ilorin, Kwara State, Nigeria.

ABSTRACT: Efficient heat removal in rotating cooling channels remains a critical challenge in thermal systems such as blades of gas turbine and rotating heat exchangers, where complex rotational forces significantly influence flow and temperature distributions. However, the combined effects of pipe eccentricity and orthogonal rotation on turbulent heat transfer in non-circular ducts are not yet fully quantified. This study numerically investigates the heat transfer characteristics of fluid flow in a straight pipe with an elliptical cross-section that rotates in an orthogonal mode. The objectives are to evaluate the influence of eccentricity, Rossby number, and Prandtl number on convective heat transfer. A three-dimensional computational fluid dynamics (CFD) model which is based on the finite volume method was developed using ANSYS Fluent. Simulations were conducted at a Reynolds number of 17,000 with a constant wall heat flux for three eccentricities (0.433, 0.866, and 0.916) and Prandtl numbers ranging from 0.73 to 7. Mesh independence was achieved at approximately 1.07×10^6 computational nodes. The results showed that the Nusselt number increased with both Rossby and Prandtl numbers, reaching a maximum value of approximately 340 at Pr = 7 and Ro = 0.1. The pipe with eccentricity 0.916 exhibited the highest heat transfer performance. The findings provide practical design guidance for cooling channels in rotating machinery such as gas turbines, heat exchangers, and rotating electrical systems.

KEYWORDS: Computational Fluid Dynamics, Elliptic Pipes, Heat Transfer, Orthogonal mode, Rotation

[Received Feb. 11, 2025; Revised Mar. 25, 2026; Accepted Mar. 27, 2026] Print ISSN: 0189-9546 | Online ISSN: 2437-2110

I. INTRODUCTION

The quest for efficient thermal management in rotating machinery remains a critical engineering challenge today in modern energy and aerospace systems. Gas turbines are used extensively in electric power generation, jet engines, and other applications. They have the ability to generate a significant quantity of useful power for a tiny size and weight, as well as long mechanical life, no reciprocating portion, and cheap maintenance costs (Cecere et al., 2023; Du et al., 2021; Mane, 2023). Enormous heat is generated in gas turbines which affect their performance efficiency, this heat must be conveyed away through cooling passages embedded in their design. As the demand for energy output is increasing, so is the need for more reliable long-term operations of gas turbine blades which are utilised in aircraft engines and electricity generation. It is well known that a higher input temperature is required to improve the efficiency of gas turbines (Xu et al., 2023; Cecere et al., 2023; Eshaghi et al., 2026; Li, Jiang, Tao, You, & Wu, 2019).

The material from which the blade is made has a thermal limit to which it can withstand (Yeranee et al., 2024). There is therefore, need to develop an enhanced effective cooling system for the turbine blade to be able to withstand the effect of thermal stress and creep among other things. The main challenge for land-based turbines is how to improve the thermal efficiency even further at the current rotor inlet temperature (Han, Dutta, & Ekkad, 2013). For instance, how can the combined cycle of large turbines be moved from 55% to 65%. Gas turbine operates at around 2000 K but these exceed the temperature to which most components can cope with (Xu et al., 2023; Li et al., 2019). It will be necessary to design an upgraded cooling system that will be able to keep the temperatures of the components within a specified range in order for them to cope with this kind of temperature. The cooling passages in a gas turbine rotor blade are made in such a way to flow either radially outward or inward (Chang et al., 2023).

Improvement in cooling of components will also bring about increased turbine efficiency as a result of coping with higher inlet temperature and as such translate into more availability of output energy at no expense (Du et al., 2021). Cooling passages are of different types; rectangular, circular and lately elliptic types are being introduced. Out of all these, the elliptic pipes display an exceptionally good fluid flow and heat transfer characteristics (Danışmaz & Akdağ, 2026). Heat transfer enhancement in rotating ducts is primarily driven by Coriolis and centrifugal forces, which induce secondary flow vortices within the ducts (Mohammad et al., 2022) . These vortices promote mixing between the warmer fluid that are close to the wall and the relatively cooler fluid at the core of the duct, thereby increasing convective heat transfer rates.

Additionally, rotation destabilizes the boundary layer at the trailing edge, resulting in increased turbulence intensity and improved heat transfer performance. The destabilisation of the boundary layer always lead to rotating duct flows producing complex secondary flows which is mostly characterised by turbulent rather than laminar flow (Martinand et al., 2023). Gas turbines must be able to endure long-term thermal and mechanical stresses, as well as fatigue, creep, and chemical deterioration, while still having a viable working life span. While it is easier to anticipate what the flow field and heat transfer in non-rotating ducts will look like, it is extremely difficult to do so in rotating passages. Coriolis forces and centripetal buoyancy affect flow in rotating channels, altering

*Corresponding author: otpopoola@unilorin.edu.ng

doi: http://doi.org/10.4314/njtd.v23i1.4498

the heat transfer properties of forced convection (Ng, 2024; Simeonov, 2024).

Many studies have been directed towards effect of rotation on enhancement of heat transfer both experimentally and numerically. You, Li, Tao, & Wei, (2018), You, Li, Wu, & Tao, (2018), Tao, Wu, You, Li, & Wei, (2018) and by Wei et al., (2017) investigated experimentally the mean flow field in a smooth rotating channel using particle image velocimetry (PIV) under the influence of buoyancy force. Sarja et al., (2020) studied numerically the use of parallel mode of rotation in negating Coriolis force effect on heat transfer. The investigation was tailored towards straight smooth pipes with imposed Reynolds number of 25,000 and Rotation numbers of 0, 0.1, 0.15, 0.2, 0.25. Results showed that there was a minor difference in the enhancement in heat transfer between leading walls and trailing walls. Dai, (2023) investigated numerically the effect on the direction of rotation axis on fluid flow at low Reynolds numbers. The angle of the rotational axis was varied from 0° to 90° while the Reynolds and Rotational numbers were varied in three steps of 300, 454 and 900 and 2,4 and 8 respectively. Results of their work showed that secondary flow is enhanced due to influence of varying the angles from 0° to 45° while the bulk velocity of the duct with aspect ratio 2.0 decreases monotonically. Sudjai et al., (2024) studied secondary flows caused by rotation in square ducts numerically. The simulation employed Large Eddy simulation model to investigate the fully developed turbulent flow in rotating and nonrotating duct. The results showed that the bottom top corner and upper lower corner of the duct wall both contain the reciprocal contribution of the convection and rotation components, according. Li, Jiang, Tao, You, & Wu, (2019) worked on the rotational effect of boundary layer flow in rectangular ducts.

The experimental investigation was geared towards the effect of orthogonal rotation on the velocity profile and shear stress of the wall. Results from the investigation showed that Coriolis force induced rotation caused a deficiency of velocity close to the leading edge of the duct and the shear stress at the zone of trailing edge is larger than that at the leading edge. The effect of heat flux under rotating condition was examined experimentally by You, Zhou, Li, & Tao, (2019). The Reynolds number of flow based mean flow velocity was 10,000 and the rotation number varied between 0 and 0.52. Results show that the displacement thickness and momentum thickness presented new changes at different radius positions consequent to heated thermal boundary layer. (Gangfu et al., 2020) in their work employed an experimental technique to quantify the instantaneous velocity and temperature fields by using a hot-wire probe with parallel-array to investigate the non-isothermal turbulent boundary layer in straight channel that is made to rotate. The Reynolds number of the flow investigated was 19000 while the rotational numbers considered were 0, 0.07, 0.21, and 0.28. Their result showed that the dimensionless temperature profile due to rotation much less than that of the static condition.

Existing literature has shown that studies on turbulent heat transfer in elliptic pipes under orthogonal rotation is limited. In particular, the influence of pipe eccentricity on heat transfer performance in rotating elliptic geometries has not been fully quantified. Moreover, the combined effects of Rossby number and Prandtl number on convective heat transfer in orthogonally mode of rotation in elliptic pipes have received little attention. Hence, the current study is geared towards addressing this gap by numerically investigating turbulent heat transfer in rotating elliptic pipes with varying eccentricity using computational fluid dynamics. The objective of the study is to evaluates the influence of pipe eccentricity, Rossby number, and Prandtl number on heat transfer. The findings of this research are expected to provide useful design guidelines for rotating cooling systems in gas turbines, heat exchangers, and other thermal engineering applications.

II. THEORETICAL ANALYSIS

A. Formulation of the Problem and Description of the Physical Model

The physical models and the cylindrical coordinates are as shown in Figure 1. It consists of a typical elliptic pipe of length *L*, semi-major and semi-minor diameters a and b respectively. The elliptic pipe is horizontal and is made to rotate with ω clock-wisely in orthogonal mode at a distance H from its rotating axis with fluid flowing through it from left to right. This is a direction perpendicular to the duct axis. While Z represents the distance from entrance of the pipe to a particular point in the axial direction, u, v, w represent the velocities along *x, y* and *z* directions.

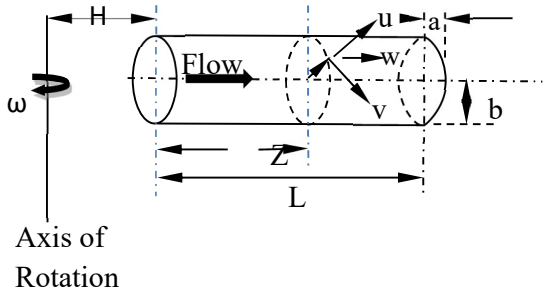

Figure 1 The physical model of horizontal elliptic pipe rotating about an orthogonal mode

B. Basic Assumptions

The pipe is thin-walled and assumed to be smooth and the working fluid is Newtonian; the forced flow is turbulent in the orthogonal mode. A constant heat flux is applied axially to the duct, and the circumferential temperature is considered to be uniform. It is assumed that the tube material's thermal conductivity is sufficient to even out circumferential variation in wall temperature. The fluid properties, with the exception of density, are constant with temperature, and there is no internal heat generation. The working fluid was assumed to be Newtonian and incompressible because most fluids used in industrial cooling systems, such as air and water, exhibit Newtonian behaviour under moderate temperature and pressure conditions. In addition, the Mach number in the present study is sufficiently low, making compressibility effects negligible.

C. Governing Equations for the Working Fluid

The fluid flow in an elliptic duct is governed by the continuity equation, Navier-Stokes equation and the energy equation as given below (Fluent, 2013):

For a steady state incompressible flow, the continuity equation which is a mathematical statement of the principle of conservation of mass is given as equation (1).

$$\nabla \bullet \rho\overrightarrow{v_r} = 0 \quad (1)$$

where $\overrightarrow{v_r} = \vec{v} - \overrightarrow{u_r}$ (2)

and $\vec{u_s} = \vec{v_t} + \vec{\omega} \times \vec{r}$ (3)

$\overrightarrow{v_r}$ is the relative velocity, $\vec{v}$ is the absolute velocity that is velocity viewed from the stationary frame, $\overrightarrow{u_s}$ is the velocity of the moving frame relative to the inertia frame and $\vec{\omega}$ the angular velocity, $\overrightarrow{v_t}$ is velocity as a function of time, ρ is the density. The momentum equation in its dimensional form for a fluid rotating at a distance from its central axis is given by Equation (4) as

$$\nabla \bullet (\rho\overrightarrow{v_r}\overrightarrow{v_r}) + \rho(2\vec{\omega} \times \overrightarrow{v_r} + \vec{\omega} \times \vec{\omega} \times r) = -\nabla P + \nabla \bullet \bar{\bar{\tau}}_r + \vec{F} \quad (4)$$

From Equation (3), the left-hand terms represent the inertia terms. For the right-hand terms, the first term represents the pressure gradient; the second term represents the viscous term and the last term, $\vec{F}$ the body force due to rotation. In Equation (4) $2\vec{\omega} \times \overrightarrow{v_r}$ represents the Coriolis acceleration term and $\vec{\omega} \times \vec{\omega} \times \vec{r}$ represents the centripetal acceleration term. $\bar{\bar{\tau}}_r$ represent the viscous stress term. If the Boussinesq approximation is valid, then the density can be written as equation (5).

$$\rho = \rho_0 + \rho_0\beta(T_w - T) \quad (5)$$

where ρ is the local density, ρ_0 is the reference density consistent with reference temperature *T*, T_w is the wall temperature and β is the cubic expansion of the fluid. The conservation of energy equation is given as equation (6)

$$\frac{\partial}{\partial t}(\rho E_r) + \nabla.(\rho\vec{v_r}H_r) = \nabla.(k\nabla T + \bar{\bar{\tau}}_r.\vec{v_r}) + S_h \quad (6)$$

where the conservation of energy equation above is given as a function of relative internal energy, E_r and relative total enthalpy, H_r with *k* being the thermal conductivity, S_h the source term. The two variables are defined by equations (7) and (8).

$$E_r = h - \frac{P}{\rho} + \frac{1}{2}(v_r^2 - u_r^2) \quad (7)$$

$$H_r = E_r + \frac{P}{\rho} \quad (8)$$

where *P* is the pressure, ∇T is the change in temperature and *h* enthalpy.

The eccentricity (*e*) of the elliptic pipe is related to the aspect ratio of a geometry by the relation in equation (9):

$$e = \sqrt{1^2 - (\frac{b^2}{a^2})} \quad (9)$$

where a and b are the minor radius and major radius of the elliptic pipe. The following non-dimensional numbers were also highlighted by (Fasquelle et al., 2014; Mahadevappa et al., 1993, 1996) and were adopted and used throughout the course of this work. The Rossby number (Ro) is the ratio of Coriolis forces to initial forces as given by equation (10).

$$Ro = \frac{\omega D_h}{V} \quad (10)$$

The Prandtl number (*Pr*) is defined as the ratio of momentum diffusivity to thermal diffusivity:

$$Pr = \frac{\vartheta}{\alpha} \quad (11)$$

The Reynolds number (Re) is the ratio of inertia forces to viscous forces given by:

$$Re = \frac{VD_h}{\vartheta} \quad (12)$$

The Nusselt number (*Nu*) is the ratio of convection heat transfer to pure conductive heat transfer.

$$Nu = \frac{hD_h}{k} \quad (13)$$

where the convection heat transfer coefficient h, at the pipe wall, and the hydraulic diameter D_h,

$$h = \frac{q''}{(T_w - T_b)} \quad (14)$$

where T_w is the temperature of the pipe wall at a given location and T_b is the bulk temperature, *q"* is the heat flux per unit area.

III. MATERIALS AND METHODS

A. Solution Technique

The numerical simulation of turbulent heat transfer in rotating elliptic pipes was carried out using the finite volume method software ANSYS Fluent (version 16.3). The geometry of the elliptic pipe was created using SolidWorks software, while grid generation was performed using ANSYS ICEM CFD. Three elliptic geometries with eccentricities of 0.433, 0.866, and 0.916 were considered in investigating the influence of pipe geometrical shape on heat transfer performance. The working fluid was assumed to be Newtonian and incompressible with constant thermophysical properties except for density variation in the buoyancy term. The flow regime was turbulent with Reynolds number fixed at 17,000 to represent practical operating conditions in rotating cooling channels of gas turbine systems. The pipe length was selected to ensure fully developed velocity and temperature profiles at the outlet. The governing equations of continuity, momentum, and energy were solved using the standard *k-ω* turbulence model, which has been widely validated for turbulent flow and heat transfer in rotating duct systems due to its computational efficiency and numerical stability. In comparison, it has been shown that k-ε turbulent model tends to over-predict heat transfer, while *k-ω* turbulent model agrees well with experimental results (Fasquelle et al., 2014).

Pressure–velocity coupling was achieved using the SIMPLE (Semi-Implicit Method for Pressure Linked Equation) scheme algorithm. Second-order upwind discretization schemes were applied to improve solution

accuracy. The convergence criteria were set at $1x10^{-6}$ for continuity and x, y and z components of the Navier-Stokes equation while $1x10^{-8}$ was used for the energy equation. These values are consistent with recommended practices for CFD simulations involving heat transfer. The pipe was assumed to rotate about an axis perpendicular to the main flow direction (orthogonal rotation), which introduces Coriolis and centrifugal forces that significantly influence flow structure and heat transfer behaviour.

B. Boundary condition

Table 1 shows the boundary conditions that were imposed during the simulation:

Table 1: Boundary Conditions Imposed on Elliptic Pipes

INLET	**Velocity inlet corresponding to Re = 1700** Inlet temperature =300 K
OUTLET	Pressure outlet = 0
WALL	No-slip condition Constant Heat flux of 1000 W/m^2
ROTATION SPEED	Rossby No. = 0-0.125

The range of Rossby number of between 0-0.125 considered in this study was selected to represent typical operating conditions encountered in rotating cooling passages of gas turbine systems. Similar Rossby number ranges have been utilised in previous experimental and numerical studies of rotating duct heat transfer (Wei et al., 2017; Sudjai et al., 2024). These values ensured stable and accurate numerical solutions.

C. Mesh Independent Study

A mesh independence study was carried out to ensure the numerical accuracy and reliability of the simulation results. Four different mesh densities were tested, which ranges from 644,000 to 1,320,000 computational nodes. The variation in the predicted Nusselt number between the fine mesh (1,068,800 nodes) and the very fine mesh (1,320,000) was less than 1%. This implies that the numerical solution had reached mesh independence. Hence, the mesh containing approximately 1,068,800 million nodes was selected for all subsequent simulations to balance computational efficiency and solution accuracy. Figure 2 shows the plot of Nu against number of nodes for the four mesh densities.

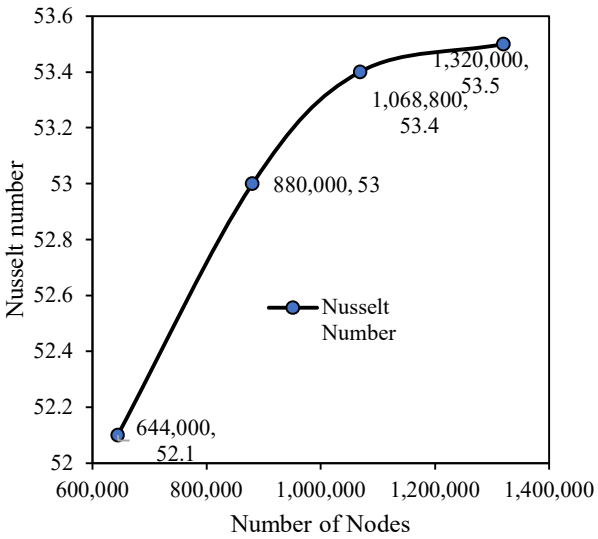

Figure 2 Nu versus Number of nodes Mesh Independent study

D. Properties of fluid and dimension of pipes

Tables 2 and 3 give the dimension of pipes and the properties of fluids used in the simulation respectively, while Figure 3 shows an elliptic pipe with mesh. He three types of fluids were selected from literature based on their use in rotary system. Fluid with Pr = 0.74 is air which is used extensively in film cooling of gas turbines (Zhu et al., 2025). Example of fluids with Pr = 4 is low viscosity organic liquids and certain refrigerants (R-134a) or high temperature heat transfer oil. An example of fluid with Pr = 7 is water. This has been employed extensively in cooling turbomachinery housing and in secondary cooling system of turbomachines.

Table 2 Dimension of Pipes employed in the study

	Eccentricity e = 0.433	**Eccentricity e = 0.866**	**Eccentricity e = 0.916**
Minor Diameter a (m)	0.011393	0.00848	0.007589
Major Diameter b (m)	0.012639	0.01697	0.0189627
Length L (m)	0.28	0.28	0.28
Distance from centre of Rotati H (m)	0.072	0.072	0.072

Table 3 Properties of fluids with *Pr* = 0.744, 7 and 4 used in the numerical work

Property	***Pr* = 0.744 (+)**	***Pr* = 7 (+)**	***Pr*=4 ***
Density, ρ (kg/m^3)	1.225	998.2	837.7
Dynamic Viscosity, μ (kg/ms)	1.7894e-05	1.003e-03	7e-04
Specific Heat at constant Pressure, C_p (J/kgK)	1006.43	4182	2701
Thermal Conductivity, k (W/mK)	0.0242	0.6000	0.4720
Thermal Expansion Coefficient, β (1/K)	3.43e-03	1.003e-03	1.911e-02

Note: Source: *(FLUENT, 2013), + (Cengel, 2004)

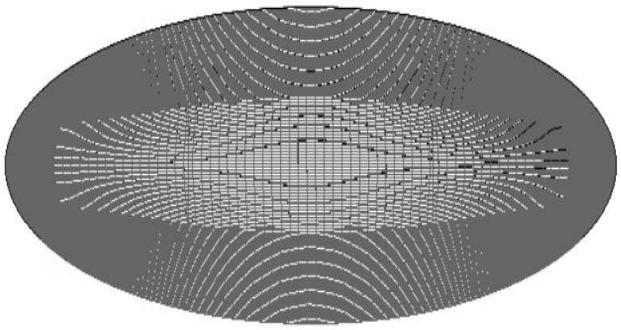

Figure 3 Elliptic Pipe with Mesh

IV. RESULTS AND DISCUSSION

Elliptic geometry of different eccentricities was investigated. These were eccentricity (e) = 0.433, 0.866 and 0.916. For the validation of the current work, the work of Baudoin, (1987), Fasquelle et al., (2014) and the current simulated work were compared whilst using the properties and physical dimensions as stated previously and explained in Tables 2. It was determined that the current work agreed within 5.3% from Baudoin, (1987). Table 4 shows the comparison between Baudoin, (1987), (Fasquelle et al., 2014) and the current work. Figure 4 gives the graphical representation of the plot for the Nusselt number against Rossby number for Baudoin (1987), (Fasquelle et al., 2014) and the current work using $k-\omega$ the turbulence model. In each case, there is a reasonable increase in heat transfer as the Rossby number (Ro) is increased. However, the graph of the current work lies in between that of Baudoin (1987) and Fasquelle et al., (2014); and the percentage difference in this case from the reference value which is Baudoin (1987) is as reported in Table 3. As was suggested by Fasquelle et al., (2014), $k-\omega$ model gave a better result than $k-\varepsilon$ model. Thus, $k-\omega$ turbulence model was used throughout this work.

Table 4 Comparison of Nusselt number (Nu) among the current work, experimental work of Baudoin (1987) and numerical work of Fasquelle et al., (2014).

	Baudoin, (1987)	Fasquelle et al., (2014)	Current work
Nu	56.4	51.8	53.4
% Difference	------	-8.2	-5.3

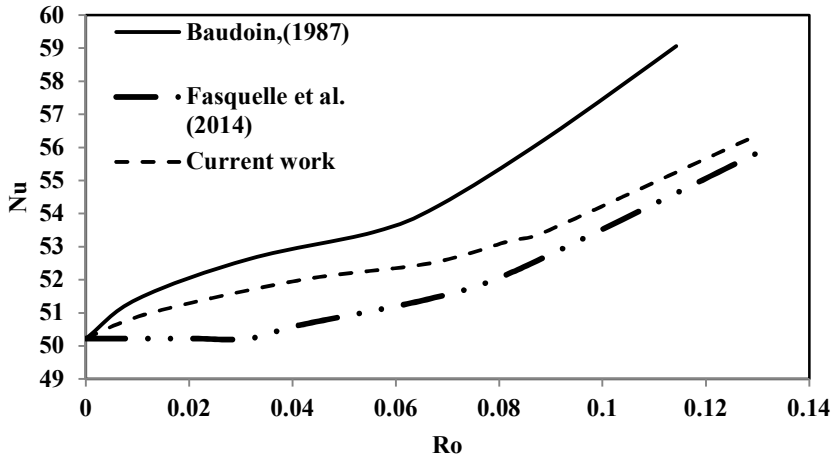

Figure 4 *Nu* versus *Ro* (*Pr*=0.73, T_w=473 K, T_{amb}= 323 K, Re=17,000, Z*=11.57, e = 0)

Figure 5 presents the mean Nusselt number (Nu) versus Rossby number (Ro) for varying eccentricities, e=0.433, 0.866 and 0.916. The Nusselt number of geometries for e=0.433 is seen to reduce with increased Rossby number up to a value of Ro=0.02 then it remained constant with increased value of Ro. The other two eccentricities, e=0.866 and e=0.916 however, are found to increase with increase in Rossby number. The increase in the Nusselt number can be adduced to the combined effect of buoyancy as result of the wall of the pipe being heated, Coriolis and centrifugal forces. As the lighter warm fluid close to the wall moves towards the inner core due to buoyancy effect, the fluid that is cooler at the core is pushed towards the wall due to the centrifugal force where it impinges on the inner wall of the pipe which translates into vigorous mixing of the fluid resulting in increased heat transfer. However, the reduction of Nu for pipe e=0.433 is as a result of

suspected flow relaminarisation whereby turbulent flow transition back to laminar flow. This is due to a rare case where the effect of rotation, Coriolis force and centrifugal forces dampens turbulence, stabilise velocity layers and reduce mixing (Scarselli et al., 2019). In the two eccentricities e=0.866 and e=0.916, rotation combined with geometry modification such has elliptic shape has been reported to enhance heat transfer (Abotsi and Kizito, 2020). What can be inferred from this is that in the case of e=0.866 and e=0.916, increasing the Rossby number increases the Nusselt number with Coriolis force improving the mixing.

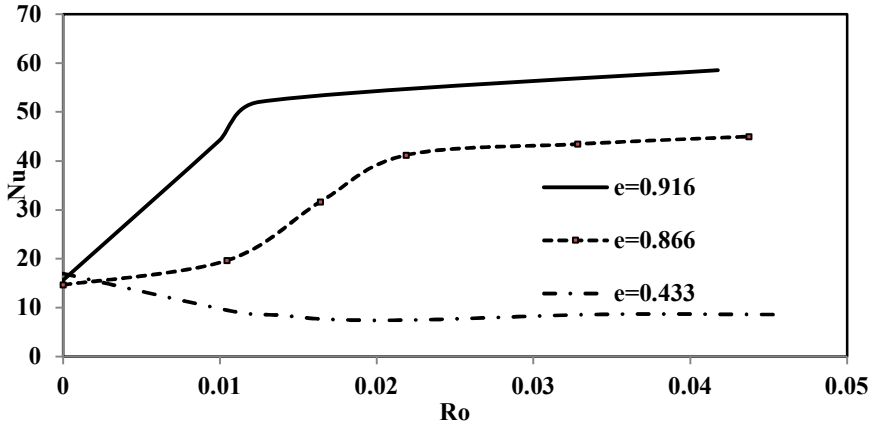

Figure 5 *Nu* versus *Ro* for three different types of geometry (*Pr*=0.73, *q''*=1,000 W, *Re*=17,000, *Z**=11.57)

Figure 6 shows the variation of temperature with dimensionless axial distance (z^+). The three geometries compared in the simulations were *e* = 0.433, 0.866 and 0.916. For each of the plots, the temperature increases gradually with dimensionless distance from 0 to around 5 in the streamwise direction. However, there is a noticeable rapid increase in temperature for pipe with eccentricity of 0.433 as from dimensionless distance of about 6 onward, this occurs in the fully developed region of flow. The observed rapid increase in temperature could be attributed to enhanced thermal boundary layer development and intensified secondary flow which was induced by rotational effects. Thus, the noticeable temperature upsurge could be as a result of increased convective heat transfer due to stronger mixing of fluid near the wall. For all the three eccentricities considered, the thermal gradients began to reduce from dimensionless distance of 5 onward leading to more stable thermal equilibrium.

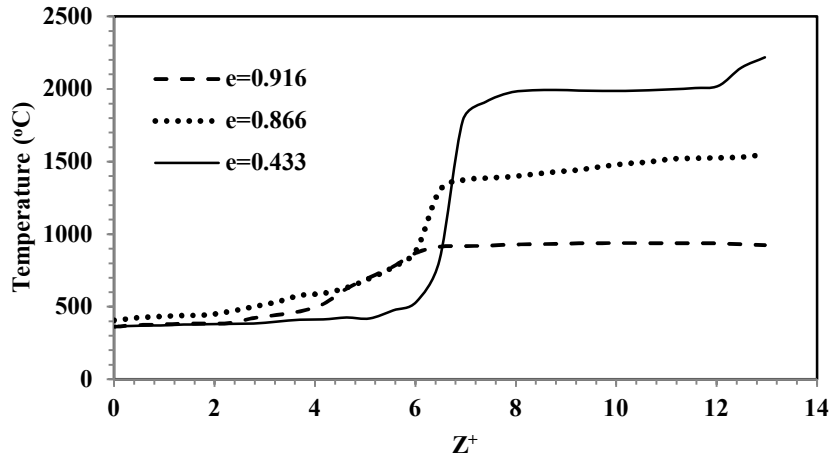

Figure 6 Temperature (ºC) versus Z^+ (*Pr*=0.73, *q''*=1,000 W,*Re*=17,000, *Ro*=0.0108)

Figure 7 shows the variation of temperature with dimensionless axial distance for leading and trailing edge of elliptic pipe with eccentricity e = 0.916. Also included in the plot is the bulk temperature of the fluid flowing in the elliptic pipe. The leading edge of the wall of the pipe was found to run at a greater temperature than the trailing edge of the wall. This is in line with the presence of Coriolis-driven cross-stream secondary flow, which enables comparatively cold fluid from the central duct region to spiral onto the trailing surface, improving cooling. Though not on the same type of geometry, the result is similar to the findings of Morris & Chang, (1997) and You, Li, Wei, & Tao, (2017). The bulk fluid temperature is at lower temperatures to both the leading and trailing edge temperatures which is similar to that of rectangular vertical duct flow in orthogonal mode as reported by Morris & Ghavami-Nasr, (1990).

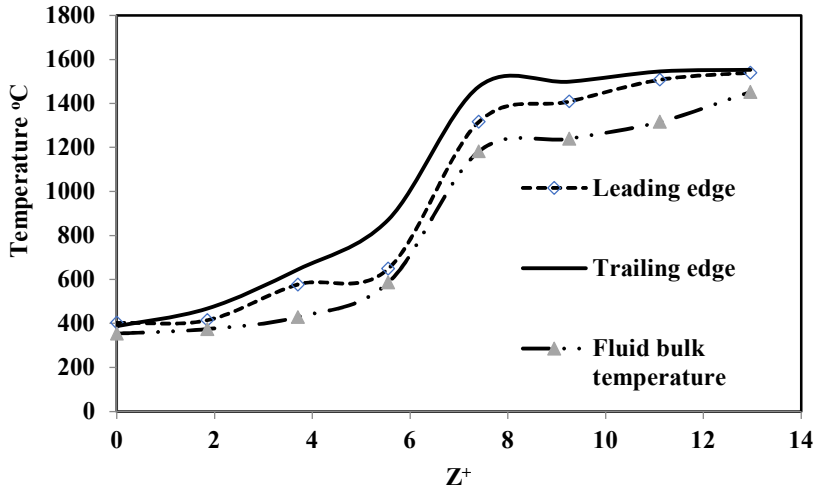

Figure 7 Temperature versus Z^+ (e=0.916, Ro=0.125, Re=17,000, q''=1,000 W, Pr=0.73)

Figure 8 presents the plot of average Nusselt number versus Rossby number for three types of fluids with Prandtl number Pr=0.73, 4 and 7. The Nusselt number of each of the fluid showed a direct positive relationship with the Rossby number. Increasing the Rossby number results in an increase in Nusselt number for each of the fluids. However, fluid with Pr=7 has the highest heat transfer followed by the fluid with Pr=4 with fluid with Pr=0.73 having the least heat transfer. The difference in heat transfer for different Prandtl numbers is as a result of Prandtl number being the ratio of momentum diffusivity over thermal diffusivity. High Prandtl number implies momentum diffuses quickly while thermal diffuse slowly and heat transfer is limited a thin layer near the wall. This translates into higher heat transfer.

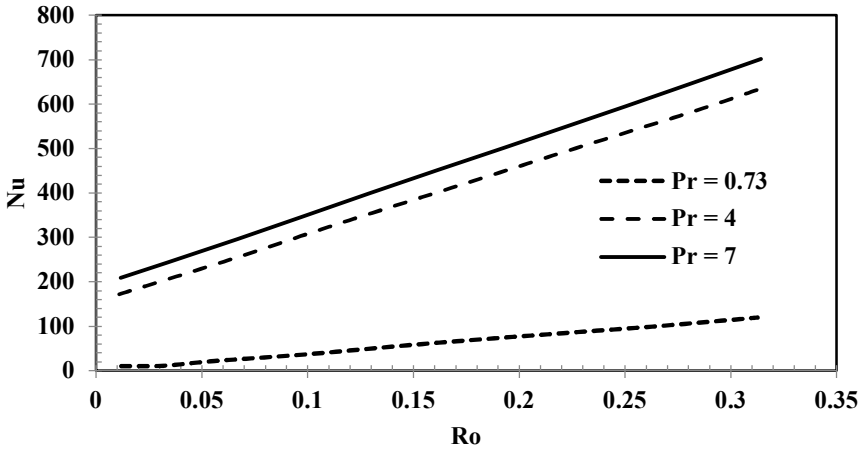

Figure 8 Nu against Ro for different types of fluids (q''=1,000W, Re=17,000, e=0.916, Z*=11.57)

Figures 9 to 13 give typical representations of the contours of temperature and velocity along axial direction of the pipe with eccentricity e=0.433, e=0.866 and e=0.916. The temperature and velocity contours exposed a clear asymmetry between the leading and the trailing edges of the pipe. For example, in Figures 9 (a) and (b), the trailing edge exhibited higher velocity and lower temperature due to the impingement of cooler fluid transported by Coriolis-induced secondary flow. This flow behaviour enhances convective heat transfer and explains the higher Nusselt number observed at the trailing edge compared to the leading edge. Similar trends have been reported in rotating duct studies where secondary flow structures significantly influence heat transfer performance (Sarja et al., 2020). The leading edge shows a higher temperature than the trailing edge. This is because as the fluid is being forced towards the trailing edge because of Coriolis effect and the centrifugal force coming into play thereby leading to the higher temperature and lower velocity. This shows that rotation has an important effect on the temperature distribution in the span-wise direction. When comparing

Figure 9 (a) to (b), it could be seen from the contours that areas of higher axial velocity in the velocity contour coincide with the zone of lower temperature. Thus, the higher velocity zone translates into lower temperature and lower velocity translates into higher temperature. This is because rotation creates stability at the leading edge while it creates instability at the trailing edge which encourages more mixing of fluids at the trailing edge and results in improved heat transfer. This

*Corresponding author: otpopoola@unilorin.edu.ng
doi: http://doi.org/10.4314/njtd.v23i1.4498

compares favourably to the observation of Li et al., ((2019) and You et al., (2019) that Coriolis forces push the velocity profile towards the trailing edge thereby causing a deficit in the leading edge.

Figures 10, and 11 show the temperature contours of elliptic pipes of eccentricities e=0.433, and 0.866 respectively. Each of the contours shows a similar pattern of the temperature being higher at the leading edge than at the trailing edge. This is similar to the same trend as reported by many researchers especially by (Morris & Chang, 1997) and Tekriwal, (1994) though both investigations were on vertical ducts in orthogonal rotation, that of (Morris & Chang, 1997) was on circular ducts while that of Tekriwal, (1994) was on rectangular duct. Cooler fluid at the centre of the elliptic pipe is heavier. The transport of this cooler fluid towards the trailing edge by Coriolis force causes secondary flow in which the flow resistance and the heat transfer is increased. The buoyancy force created by the action of heating of the wall tends to move the warmer fluid at the wall towards the centre. This as a result of collision between the warmer and the cooler fluids which also cause vigorous mixing and translate into increased heat transfer.

Figures 12 and 13 show the velocity contours of the elliptic pipes of eccentricities under consideration. On close observation, it could be seen that the lowest velocity attained in each of the pipes is seen at the leading edge while the higher velocities are relatively seen at the trailing edge. This is as result of Coriolis force with the attendance effect of transporting the fluid towards the trailing edge.

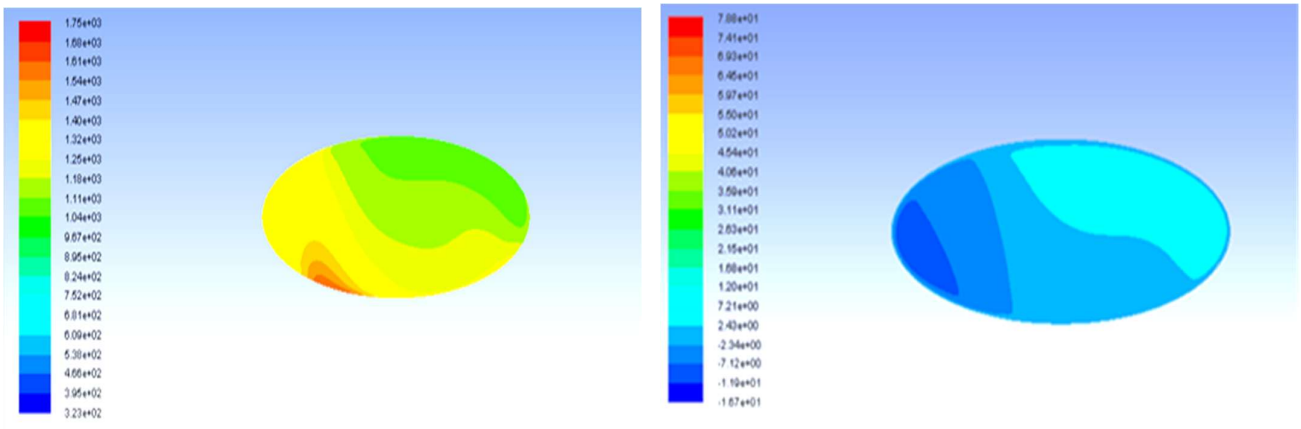

(a) (b)

Figure 9 Typical contour representation for elliptic pipe e=0.916 (a) temperature (b) Axial velocity (Ro=0.125, Re=17,000, q''=1,000 W/m^2, Pr=0.73, Z*=11.57)

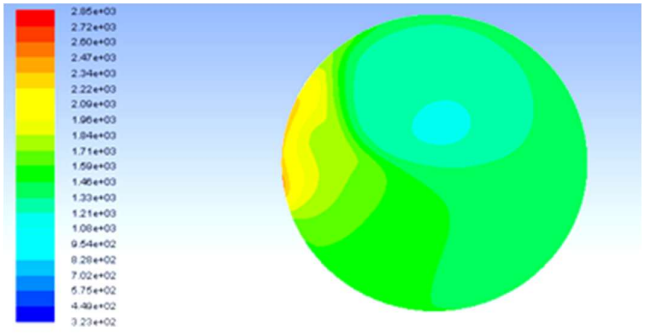

Figure 10 Typical Temperature contour for elliptic pipe e = 0.433 0.125, *Re* = 17,000, *q''*=1,000 W/m^2, *Pr* = 0.73, *Z**=11.57)

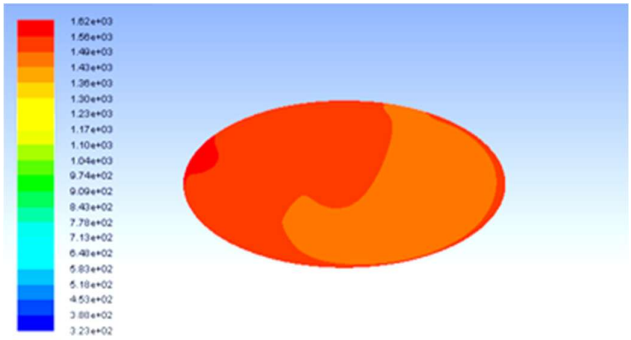

Figure 11 Typical Temperature contour for elliptic pipe *e*= 0.866 (*Ro* = 0.125, Re =17,000, *q'*=1,000 W/m^2, *Pr* = 0.73, *Z**=11.57)

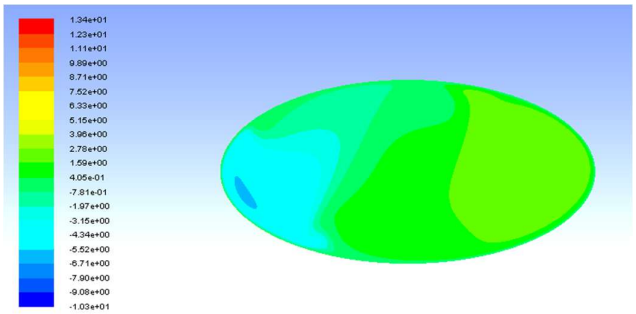

Figure 12 Typical velocity contour for elliptic pipe e=0.866 (Ro=0.125, Re=17,000, q''=1,000 W/m^2, Pr=0.73,

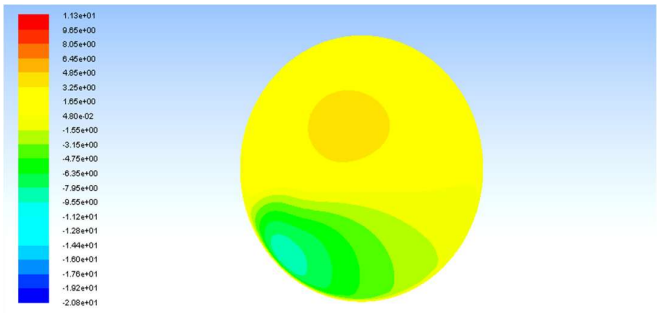

Figure 13 Figure 13: Typical velocity contour for elliptic pipe e=0.433 (Ro=0.125, Re=17,000, q''=1,000 W/m^2, Pr=0.73,

V. CONCLUSION

A numerical investigation on heat transfer and fluid flow in elliptic pipe has been conducted using commercially available software Ansys Fluent. The results of the study demonstrated that rotation significantly enhances convective heat transfer in elliptic pipes due to the development of secondary flow structures with pipe of eccentricity e=0.916 being the most suitable for cooling out of the eccentricities considered. However, practical implementation should consider additional factors such as pressure drop, manufacturing complexity, and structural integrity. The fluid with maximum heat transfer among those studied was Pr=7. Fluid with Pr=7 gave the highest heat transfer of Nu=340. Rotation improves heat transfer and increase in Ro enhanced heat transfer with the trailing edge having higher Nu than the leading edge for orthogonal mode rotation. The findings provide useful design guidance for rotating cooling channels in gas turbine systems and other thermal engineering applications. Improved heat transfer performance in elliptic pipes can be used to enhance cooling efficiency in gas turbine blades, rotating heat exchangers, and industrial cooling systems. By optimizing pipe geometry and rotational speed, engineers can achieve higher thermal efficiency while minimizing energy consumption and material stress.

AUTHOR CONTRIBUTIONS

O.T. Popoola: Conceptualization, Software, Simulation, Validation, Writing - original draft, Writing - review & editing,. O.A. Lasode: Conceptualization, Methodology, review & editing; I. K. Adegun: Writing-review, Validation; A. B. Rabiu: Writing - review & editing.

REFERENCES

Abotsi, O. Y. W., & Kizito, J. P. (2020). Turbulent heat transfer in an axially rotating pipe at high rotation rate: A numerical study. *Frontiers in Heat and Mass Transfer*, 14, 1–6. https://doi.org/10.5098/hmt.14.24.

Baudoin, B. (1987). Contribution à l'étude des conditions d'écoulement dans le circuit de refroidissement d'un moteur électrique de type ouvert (Doctoral dissertation, Poitiers).

Cecere, D., Giacomazzi, E., Di Nardo, A., & Calchetti, G. (2023). Gas Turbine Combustion Technologies for Hydrogen Blends. *Energies*, 16(19), 6829. https://doi.org/10.3390/en16196829.

Chang, S. W., Wu, P. S., Wan, T. Y., & Cai, W. L. (2023). A Review of Cooling Studies on Gas Turbine Rotor Blades with Rotation. *Inventions*, 8(1), 21. https://doi.org/10.3390/inventions8010021.

Dai, Y. J. (2023). Effects of the direction of rotation axis on turbulent flows in rectangular ducts. *Physics of Fluids*, 35(9). https://doi.org/10.1063/5.0156921.

Danışmaz, M., & Akdağ, Ü. (2026). Enhancing heat transfer performance in elliptical tubes with nano fluids: A numerical case study. *Numerical Heat Transfer, Part A: Applications*. https://doi.org/10.1080/10407782.2025.2525315.

Du, W., Luo, L., Jiao, Y., Wang, S., Li, X., & Sunden, B. (2021). Heat transfer in the trailing region of gas turbines – A state-of-the-art review. *Applied Thermal Engineering*, 199(July), 117614. https://doi.org/10.1016/j.applthermaleng.2021.117614.

Fasquelle, A., Pellé, J., Harmand, S., & Shevchuk, I. V. (2014). Numerical study of convective heat transfer enhancement in a pipe rotating around a parallel axis. *Journal of Heat Transfer*, 136(5). https://doi.org/10.1115/1.4025642/373612.

Fluent, A. (2013). Ansys Fluent Theory Guide. ANSYS Inc., USA, 15317(November), 724–746.

Gangfu, L., Haiwang, L., Ruquan, Y., Huijie, W., Zhi, T., & Shuangzhi, X. (2020). Experimental Investigation on Velocity and Temperature Field in a Rotating Non-isothermal Turbulent Boundary Layer using Hot-wire. *Scientific Reports*, 10(1), 1–15. https://doi.org/10.1038/s41598-020-66853-6.

Han, J. C., Dutta, S., & Ekkad, S. (2013). Gas Turbine Heat Transfer and Cooling Technology. In Proceedings of the National Heat Transfer Conference (2nd ed., Vol. 2). Taylor and Francis Group.

Li, H., Jiang, Z., Tao, Z., You, R., & Wu, H. (2019). Effect of system rotating on turbulent boundary layer flow. *International Journal of Heat and Fluid Flow*, 75(January), 185–194. https://doi.org/10.1016/j.ijheatfluidflow.2019.01.003

Mahadevappa, M., Rammohan Rao, V., & Sastri, K, V. M. (1996). Numerical Study of Steady Laminar Fully Developped Fluid Flow and Heat Transfer in Rectangular and Elliptical Ducts Rotating about a Parallel Axis. *International Journal of. Heat and Mass Transfer*, 39(4), 867–875.

Mahadevappa, M., Rao, K. V. C., & Sastri, V. M. K. (1993). Experimental Investigation for Fluid Flow and Heat Transfer in an Elliptical Duct Rotating about Parallel Axis. *Experimental Heat Transfer*, 6(2), 97–109. https://doi.org/10.1080/08916159308946448.

Mane, S. (2023). Advancements in Gas Turbine Engine Technology: A Conceptual Aspect. *International Journal of Enhanced Research in Science*, 12(7), 2319–7463. https://www.researchgate.net/publication/372317273.

Martinand, D., Serre, E., & Viaud, B. (2023). Instabilities and routes to turbulence in rotating disc boundary layers and cavities. Philosophical Transactions of the Royal Society A: Mathematical, *Physical and Engineering Sciences*, 381(2243). https://doi.org/10.1098/rsta.2022.0135.

Mohammad, Z. I., Rabindra, N. M., & Suvash, C. S. (2022). Impacts of Rotation on Unsteady Fluid Flow and Energy Distribution through a Bending Duct with Rectangular Cross Section. *Energy Engineering*, 119(2), 453–472. https://doi.org/10.32604/ee.2022.018160.

Morris, W. D., & Chang, S. W. (1997). An experimental study of heat transfer in a simulated turbine blade cooling passage. *International Journal of Heat and Mass Transfer*, 40(15), 3703–3716. https://doi.org/10.1016/S0017-9310(96)00311-0.

Ng, C. K. (2024). Simple quantitative examples illustrating how the centrifugal and Coriolis forces 'rescue' Newton's second law in rotating frames. *Physics Education*, 59(3), 035001. https://doi.org/10.1088/1361-6552/AD2AF2.

Sarja, A., Singh, P., & Ekkad, S. V. (2020). Parallel rotation for negating Coriolis force effect on heat transfer. *Aeronautical Journal*, 124(1274), 581–596. https://doi.org/10.1017/aer.2020.1

Scarselli, D., Kühnen, J., & Hof, B. (2019). Relaminarising pipe flow by wall movement. *Journal of Fluid Mechanics*, 867, 934–948. https://doi.org/10.1017/jfm.2019.191.

Simeonov, L. S. (2024). Intuitive Derivation of the Coriolis Force. https://arxiv.org/pdf/2409.14135.

Sudjai, W., Juntasaro, V., & Juttijudata, V. (2024). Mechanisms of Secondary Flows in a Straight Square Duct under the Effect of Rotation. *Engineering Journal*, 28(5), 53–71. https://doi.org/10.4186/ej.2024.28.5.53.

Tao, Z., Wu, H., You, R., Li, H., & Wei, K. (2018). Turbulent characteristics and rotation correction of wall function in rotating channel with high local rotation parameter. *Chinese Journal of Aeronautics,* 31(10), 1985–1999. https://doi.org/10.1016/j.cja.2018.08.006.

Tekriwal, P. (1994). Heat transfer predictions with extended k-ε turbulence model in radial cooling ducts rotating in orthogonal mode. *Journal of Heat Transfer*, 116(2), 369–380. https://doi.org/10.1115/1.2911409.

Wei, K., Tao, Z., Wu, H., Xu, G., Li, H., & You, R. (2017). Interaction between the primary flow fields and the secondary flow fields under rotating condition. *Experimental Thermal and Fluid Science*, 84, 217–230. https://doi.org/10.1016/j.expthermflusci.2017.02.010.

Xu, L., Sun, Z., Ruan, Q., Xi, L., Gao, J., & Li, Y. (2023). Development Trend of Cooling Technology for Turbine Blades at Super-High Temperature of above 2000 K. *Energies*, 16(2), 668. https://doi.org/10.3390/en16020668.

Yeranee, K., Rao, Y., Xu, C., Zhang, Y., & Su, X. (2024). Turbulent Flow Heat Transfer and Thermal Stress Improvement of Gas Turbine Blade Trailing Edge Cooling with Diamond-Type TPMS Structure. *Aerospace,* 11(1). https://doi.org/10.3390/aerospace11010037.

You, R., Li, H., Tao, Z., & Wei, K. (2018). Measurement of the mean flow field in a smooth rotating channel with coriolis and buoyancy effects. *Journal of Turbomachinery*, 140(4). https://doi.org/10.1115/1.4038870.

You, R., Li, H., Wei, K., & Tao, Z. (2017). Two-dimensional heat transfer distribution in a rotating smooth rectangular channel with four surface heating boundary condition. *Advances in Mechanical Engineering*, 9(10), 1–15. https://doi.org/10.1177/1687814017733243.

You, R., Li, H., Wu, H., & Tao, Z. (2018). PIV flow measurements for a rotating square smooth channel heated by basically uniform heat flux. *International Journal of Heat and Mass Transfer*, 119, 236–246. https://doi.org/10.1016/j.ijheatmasstransfer.2017.11.073.

You, R., Zhou, S., Li, H., & Tao, Z. (2019). Effect of heat flux on boundary layer flow under rotating conditions. *International Journal of Heat and Fluid Flow*, 80(October), 108493. https://doi.org/10.1016/j.ijheatfluidflow.2019.108493.

Zhu, S., Li, Y., Yan, J., & Zhang, C. (2025). Recent Advances in Cooling Technology for the Leading Edge of Gas Turbine Blades. *Energies*, 18(3), 540. https://doi.org/10.3390/en18030540.